Supplemental Information: The topological invariants of rotationally symmetric crystals

Jans Henke,[1] Mert Kurttutan,[1] Jorrit Kruthoff,[2] and Jasper van Wezel[1,*]

[1] *Institute for Theoretical Physics Amsterdam and Delta Institute for Theoretical Physics, University of Amsterdam, Science Park 904, 1098 XH Amsterdam, The Netherlands*

[2] *Stanford Institute for Theoretical Physics, Stanford University, Stanford, CA 94305*

Appendix A: Topological invariants in the concentric Wilson loop spectrum

Following the arguments in Refs. [1–4], we define the Wilson loop operator as a matrix-valued one-form for a given path $\mathcal{C}$ and Berry connection $\mathbf{A}(\mathbf{k})$:

$$\mathcal{W}(\mathbf{k}_0,\mathcal{C}) = \mathcal{P}\exp\left(i\oint_{\mathcal{C}} d\mathbf{k}\cdot\mathbf{A}(\mathbf{k})\right). \tag{A1}$$

Here, $\mathcal{P}$ denotes path-ordering, $\mathbf{k}_0$ is a base point of $\mathcal{C}$, and the Berry connection has matrix elements $\mathbf{A}_{mn}(\mathbf{k}) = i\langle u_m(\mathbf{k})|\nabla_k|u_n(\mathbf{k})\rangle$. It can be readily checked that the Berry connection is a skew-Hermitian matrix, rendering the Wilson loop a unitary operator.

Under a unitary symmetry $g \in G$ the Wilson loop matrix elements transform as:

$$g : \mathcal{W}_{ij}(\mathbf{k}_0,\mathcal{C}) \to D^l_i(g,\mathbf{k}_0)\mathcal{W}_{lk}(g\cdot\mathbf{k}_0, g\cdot\mathcal{C})D^k_j(g,\mathbf{k}_0)^*. \tag{A2}$$

Here $D^i_l(g,\mathbf{k}_0)$ is the representation of the symmetry g, which could depend on base point $\mathbf{k}_0$. If $\mathcal{C}$ is a closed loop, the two D's in this expression have the same $\mathbf{k}_0$ argument, while for a line it would be the the beginning and end point, respectively on the right and left. Invariance under a unitary symmetry thus means

$$\mathcal{W}_{ij}(\mathbf{k}_0,\mathcal{C}) = D^l_i(g,\mathbf{k}_0)\mathcal{W}_{lk}(g\cdot\mathbf{k}_0, g\cdot\mathcal{C})D^k_j(g,\mathbf{k}_0)^*. \tag{A3}$$

In the presence of TRS and additional symmetries, two types of choices for $\mathcal{C}$ are noteworthy. These are non-contractible cycles around the BZ (the type most commonly considered in the literature [1, 3–5]) and loops that enclose high symmetry points (see also [4]). The latter type can be chosen to be invariant under time-reversal symmetry. The loops around high-symmetry points can be considered non-contractible, because the high-symmetry points are fixed points of the spatial symmetries.

To see how TRS affects the Wilson loop operators along these two types of non-contractible loops, we first discretize the Wilson loop, implementing the path-ordering explicitly. The curve $\mathcal{C}$ specifies a path in the BZ that can be parametrized by $\mathbf{k}(t)$ with $0 \le t \le 1$ and $\mathbf{k}(0) = \mathbf{k}_0 = \mathbf{k}(1)$ (up to a reciprocal lattice vector). Conventionally, we will take $\mathbf{k}(t)$ decreasing with t, so we go around $\mathcal{C}$ in a clockwise direction. We discretize the curve by considering discrete values $t_i = i/N$ with $i = 1, 2, \dots N$ and N large. Denoting $\mathbf{k}_i$ the momentum at $t = t_i$, we then have:

$$\begin{aligned}\mathcal{W}_{mn}(\mathbf{k}_0,\mathcal{C}) &= \left[\mathcal{P}\exp\left(i\oint_{\mathcal{C}} d\mathbf{k}\cdot\mathbf{A}(\mathbf{k})\right)\right]_{mn} \\ &\approx \sum_{j_1,j_2,\dots j_N} (\delta_{mj_1} + i\,d\mathbf{k}_1\cdot\mathbf{A}_{mj_1}(\mathbf{k}_0))(\delta_{j_1j_2} + i\,d\mathbf{k}_2\cdot\mathbf{A}_{j_1j_2}(\mathbf{k}_1))\cdots(\delta_{j_Nn} + i\,d\mathbf{k}_N\cdot\mathbf{A}_{j_Nn}(\mathbf{k}_{N-1})).\end{aligned} \tag{A4}$$

Here we used $d\mathbf{k}_i \equiv \mathbf{k}_{i-1} - \mathbf{k}_i$. Using the definition of the Berry connection, we can write $\delta_{mn} - i\,(\mathbf{k}_i - \mathbf{k}_{i-1})\cdot\mathbf{A}_{mn}(\mathbf{k}_i) \approx \langle u_m(\mathbf{k}_{i-1})|u_n(\mathbf{k}_i)\rangle$. Taking $N\to\infty$ and keeping only terms linear in $d\mathbf{k}_i$, we then find:

$$\mathcal{W}_{mn}(\mathbf{k}_0,\mathcal{C}) = \lim_{N\to\infty}\langle u_m(\mathbf{k}_0)|\prod_{i=1}^{N} P(\mathbf{k}_i)|u_n(\mathbf{k}_0)\rangle\,. \tag{A5}$$

* vanwezel@uva.nl

Here, the product is path-ordered around $\mathcal{C}$ and the projectors are defined as $P(\mathbf{k}_i) = \sum_j |u_j(\mathbf{k}_i)\rangle \langle u_j(\mathbf{k}_i)|$.

To find the action of time-reversal symmetry on this representation of the Wilson loop operator, recall that time-reversal maps states at $\mathbf{k}$ onto states at $-\mathbf{k}$. We may therefore write a Bloch state at $-\mathbf{k}$ in terms of time-reversed Bloch states at $\mathbf{k}$:

$$|u_n(-\mathbf{k})\rangle = \sum_m D_{nm}(\mathbf{k}) T |u_m(\mathbf{k})\rangle \tag{A6}$$

Here, the time reversal operator T includes complex conjugation and D is a unitary matrix. Using this relation, the projectors P at $-\mathbf{k}$ can also be related to ones at $\mathbf{k}$:

$$\begin{aligned} P(-\mathbf{k}) &= \sum_{j,m,m'} D_{jm}(\mathbf{k}) T |u_m(\mathbf{k})\rangle \langle u_{m'}(\mathbf{k})| T^\dagger (D_{m'j})^*(\mathbf{k}) \\ &= -\sum_m T |u_m(\mathbf{k})\rangle \langle u_m(\mathbf{k})| T^{-1} \\ &= -TP(\mathbf{k})T^{-1}. \end{aligned} \tag{A7}$$

Here we used the fact that T is anti-unitary, such that $T^\dagger = -T^{-1}$. If we now consider a loop $\mathcal{C}$ that is time-reversal symmetric, then:

$$T\mathcal{W}(\mathbf{k}_0, \mathcal{C})T^{-1} = \mathcal{W}(-\mathbf{k}_0, \mathcal{C}), \tag{A8}$$

To see this explicitly, take for example four points $\mathbf{k}_j$, $j = 0, 1, 2, 3$, on the unit circle in $\mathbf{k}$-space, equally spaced. Under T we then have $\mathbf{k}_j \to \mathbf{k}_{j+2}$, so the discrete Wilson loop $\mathcal{W} = P(\mathbf{k}_0)P(\mathbf{k}_1)P(\mathbf{k}_2)P(\mathbf{k}_3)$ gets mapped to:

$$T\mathcal{W}T^{-1} = TP(\mathbf{k}_0)T^{-1}TP(\mathbf{k}_1)T^{-1}TP(\mathbf{k}_2)T^{-1}TP(\mathbf{k}_3)T^{-1} = P(\mathbf{k}_2)P(\mathbf{k}_3)P(\mathbf{k}_0)P(\mathbf{k}_1). \tag{A9}$$

This is the same discrete Wilson loop, with the four points rotated but their order remaining the same.

For a rotation symmetry C_n we analogously find:

$$C_n\mathcal{W}(\mathbf{k}_0, \mathcal{C})C_n^{-1} = \mathcal{W}(g \cdot \mathbf{k}_0, g \cdot \mathcal{C}), \tag{A10}$$

in agreement with the expression in Eq. A2. If we consider a loop for which the base-point dependence is only through its length $|\mathbf{k}_0|$, the minus sign in $-\mathbf{k}_0$ is irrelevant. This is the case for two-dimensional loops that are rotationally symmetric.

To relate these results to previous literature, notice that often loops around non-contractible cycles are considered, and that those loops are in general neither invariant under rotations, nor time-reversal symmetric. In particular for the action of time-reversal symmetry, this means that for such loops we have:

$$T\mathcal{W}(\mathbf{k}_0, \mathcal{C})T^{-1} = \mathcal{W}(-\mathbf{k}_0, \mathcal{C}_r) = \mathcal{W}(-\mathbf{k}_0, \mathcal{C})^\dagger. \tag{A11}$$

Here $\mathcal{C}_r$ is the orientation-reversed loop. That the orientation is reversed under time-reversal can be easily seen by considering for example a curve at constant k_x.

Now let us consider systems with both C_3 and T symmetry, and consider a path $\mathcal{C}$ tracing out a hexagon centered at Γ with size $|\mathbf{k}_0|$. We denote the loop by $\mathcal{C}_h$. Imposing invariance under time-reversal and three-fold rotation, we then have the constraints:

$$T\mathcal{W}(|\mathbf{k}_0|, \mathcal{C}_h)T^{-1} = \mathcal{W}(|\mathbf{k}_0|, \mathcal{C}_h), \quad C_3\mathcal{W}(|\mathbf{k}_0|, \mathcal{C}_h)C_3^{-1} = \mathcal{W}(|\mathbf{k}_0|, \mathcal{C}_h). \tag{A12}$$

We can choose a gauge in which $T = i\sigma_y K$ and $C_3 = e^{\sigma_z i\pi/3}$, and consider the $U(2)$ Wilson loop of a single Kramers pair. The unitary matrix $\mathcal{W}$ can then be written as:

$$\mathcal{W}_h(\mathbf{k}_0) = \mathcal{W}(|\mathbf{k}_0|, \mathcal{C}_h) = \begin{pmatrix} a(\mathbf{k}_0) & b(\mathbf{k}_0) \\ c(\mathbf{k}_0) & d(\mathbf{k}_0). \end{pmatrix} \tag{A13}$$

The symmetry constraints on the matrix elements then become:

$$a(\mathbf{k}_0) = d^*(-\mathbf{k}_0), \quad b(\mathbf{k}_0) = -c^*(-\mathbf{k}_0), \quad a(\mathbf{k}_0) = a(g \cdot \mathbf{k}_0), \quad b(\mathbf{k}_0) = b(g \cdot \mathbf{k}_0)e^{-2\pi i/3} \tag{A14}$$

Here, g is the action of the three-fold rotation symmetry on k-space. The first two constraints come from time-reversal symmetry, while the latter two arise from the three-fold rotational symmetry. The Wilson loop only depends on the

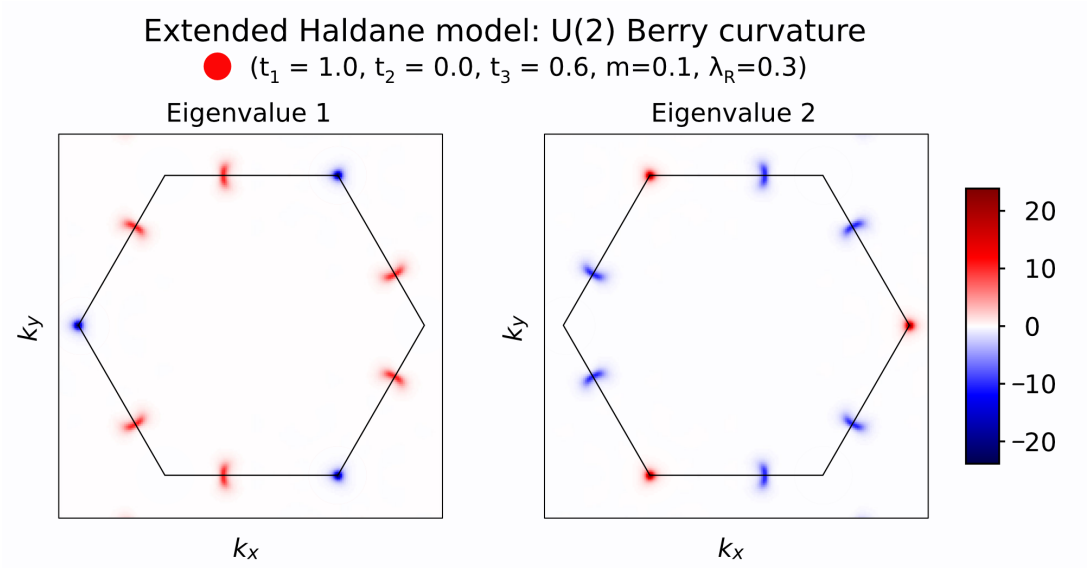

Figure A.1. $U(2)$ Berry curvature of the extended Haldane model (see main text). The black hexagons indicate the size of the BZ. The parameters chosen here correspond to the red circle in Figure 2a. The curvature was computed as a grid of 200×200 square Wilson loops covering the area shown above.

length of $\mathbf{k}_0$, and since $|g \cdot \mathbf{k}_0| = |\mathbf{k}_0|$, b must vanish in our chosen gauge. This means c also vanishes and $d = a^*$. Furthermore, since the matrix $\mathcal{W}(\mathbf{k}_0)$ must be unitary, the $a(|\mathbf{k}_0|)$ must be a pure phase $e^{i\theta(|\mathbf{k}_0|)}$. The Wilson loop operator thus reduces to:

$$\mathcal{W}_h(\mathbf{k}_0) = \mathcal{W}_h(|\mathbf{k}_0|) = \begin{pmatrix} e^{i\theta(|\mathbf{k}_0|)} & 0 \\ 0 & e^{-i\theta(|\mathbf{k}_0|)} \end{pmatrix} = e^{i\sigma_z\theta(|\mathbf{k}_0|)}. \tag{A15}$$

Because the Wilson loop operator is the exponent of only a single Pauli matrix, its eigenvalues are always complex conjugates and linear crossings of eigenvalues $\theta(|k \approx k_*|) = a + b(k - k_*) + \dots$ with $a \in \{0, \pm\pi\}$ are protected. This means that they can be gapped only by adding additional Pauli matrices that break either the T or C_3 symmetry, or by having the coefficient b vanish. The latter mechanism requires either two linear crossings to merge and annihilate, or a complete vanishing of the k-dependence of $\theta(k)$.

Importantly, a full hexagonal Wilson loop contains redundant information due of the symmetries of the system, such that not all protected degeneracies in its spectrum are relevant. To extract meaningful topological information from a concentric WLS based on these types of loops, one must consider the concentric WLS of a single fundamental domain of the BZ, as defined by the symmetries. To determine what constitutes a fundamental domain, it is helpful to consider an infinitesimal Wilson loop, i.e. the $U(2)$ Berry curvature $\mathcal{F}_W$, at an arbitrary point $\mathbf{k}$ in the BZ. Note that the eigenvalues of such a generic infinitesimal loop are not constrained to be complex conjugates. Threefold rotational symmetry ensures that $\mathcal{F}_W(\mathbf{k}) = \mathcal{F}_W(g \cdot \mathbf{k})$, while TRS ensures that $\mathcal{F}_W(\mathbf{k}) = \mathcal{F}_W(-\mathbf{k})^\dagger$. That is, the curvature eigenvalues of either of the two states in the Kramers pair considered are three-fold symmetric, and the curvature of one of the two bands is inverted with respect to the other (see Figure A.1). It then follows that neighbouring sextants of the BZ (may) have different curvatures, requiring the combination of two sextants of the BZ to capture all the symmetry-allowed information. From this we conclude that the fundamental domain of a $p3$ system covers two inequivalent sextants, and the relevant topological information can be extracted from one third of the full hexagonal WLS. More generally, for a system with (only) n-fold rotational symmetry, the fundamental domain constitutes $1/n^{\text{th}}$ of the BZ.

Finally, one should note that a trivial Wilson loop spectrum, i.e. one starting and ending at zero, without crossing $\theta = \pi$ in between, is allowed by symmetry to flatten entirely, thus removing any crossings at $\theta = 0$. As noted above, this corresponds to tuning the prefactor b of the linear term in an expansion around the crossing point to zero. This complete flattening is only allowed for trivial spectra, but zero-crossings in any spectrum may be removed upon addition of a trivial Kramers pair, as explained in Appendix B. In that sense, zero-crossings are "fragile" [3, 4, 6, 7]. Because the starting point of a concentric spectrum is fixed to $\theta = 0$, π-crossings do not have the same fragility, and can only be removed by either breaking a symmetry or closing the spectral gap. Thus, we conclude that both the winding (FKM invariant) and the parity of π-crossings in a concentric WLS covering a fundamental domain of the BZ, constitute topological invariants.

Appendix B: Multiple occupied bands and elementary spectra

Having found that the parity of crossings of eigenvalues at $\theta = \pi$ in a concentric WLS cannot be changed without breaking either TRS or rotational symmetry, we must ensure that this feature is also robust upon the addition of topologically trivial TRS-related pairs of bands (Kramers pairs). It is important to note here that when there are multiple occupied Kramers pairs, in the presence of only time-reversal and pure rotational symmetries, one can always consider the $U(2)$ WLS of each separate Kramers pair. If two Kramers pairs overlap, such that the identification of band indices is non-trivial, it is always possible to perturb the system without breaking any symmetries and separate the overlapping pairs. Each individual $U(2)$ WLS is subject to the symmetry restrictions discussed in Appendix A, and can be assigned its own topological invariants.

Adiabatic deformations of the WLS of an individual Kramers pair will not change the topological indices associated with that spectrum. However, some (quantised) amount of $U(2)$ Berry curvature in one Kramers pair may transfer to another occupied pair as crossings between two $U(2)$ WLS open up a gap. Different combinations of spectra for multiple occupied Kramers pairs may therefore represent the same combined topological phase (see Fig. B.1). By simply summing the topological invariants extracted from each occupied Kramers pair's concentric WLS and (where applicable) line invariants, one can obtain the total topological classification of any Hamiltonian with T and C_n symmetries.

The blue spectra in Fig. B.1 demonstrate that a concentric WLS in $p3$ that winds to $10\pi/3$ and one that winds to $2\pi/3$ both carry topological indices $(1, 0)$. In the same way, a $(0, 0)$ spectrum that does not wind is topologically equivalent to one that winds to 4π. More generally, the topological invariants extracted from concentric WLS are cyclic, and whenever a spectrum contains multiple π-crossings, these crossings can pairwise annihilate upon the addition of a trivial Kramers pair. We shall call the spectra that remain unchanged upon hybridisation with a trivial WLS "elementary spectra". In systems with two, three, four, or six-fold rotational symmetry, one finds 4, 4, 6, and 8 elementary spectra, respectively, as shown in Fig. B.2.

One should note that although the elementary WLS always correspond to a unique set of w_{FKM} and w_π invariants, the opposite is not true. For example, in $p6$ there are two elementary spectra for each combination of the two invariants. Each of these pairs of elementary WLS can be transformed into one another upon hybridization with a specific non-trivial additional Kramers pair. In $p4$ the same doubling of spectra corresponding to a set of invariants occurs for a subset of the elementary WLS.

To complete the evaluation of all the topological invariants for a TRS system with rotational symmetry, the WLS in some cases needs to be augmented by line invariants. In $p2$, the $\mathbb{Z}_2^4$ classification is determined by two independent LBO line invariants, the FKM invariant, and the new w_π invariant. The latter two can be evaluated directly from the concentric WLS, where the four elementary spectra describe two independent $\mathbb{Z}_2$ invariants, while the line invariants are the eigenvalues of two additional Wilson loops along ΓXΓ and ΓYΓ. In $p3$, there are no line invariants, so the full classification is $\mathbb{Z}_2^2$ which is fully determined by w_{FKM} and w_π extracted from the concentric WLS. (Note that this corrects a statement in [8]: although the $U(1)$ vortices discussed there cannot be moved away from K, they can be smeared in a C_3 and TRS invariant fashion, leaving two rather than three $\mathbb{Z}_2$ invariants.) In $p4$, one expects a $\mathbb{Z}_2^3$ classification [8], where only one independent LBO line invariant remains, which can be combined with the w_{FKM} and w_π extracted from the six elementary WLS. Finally, in $p6$ we expect a classification of $\mathbb{Z}_2^3$ [8], where the third invariant is the LBO invariant along the C_2 and time-reversal invariant line ΓMΓ.

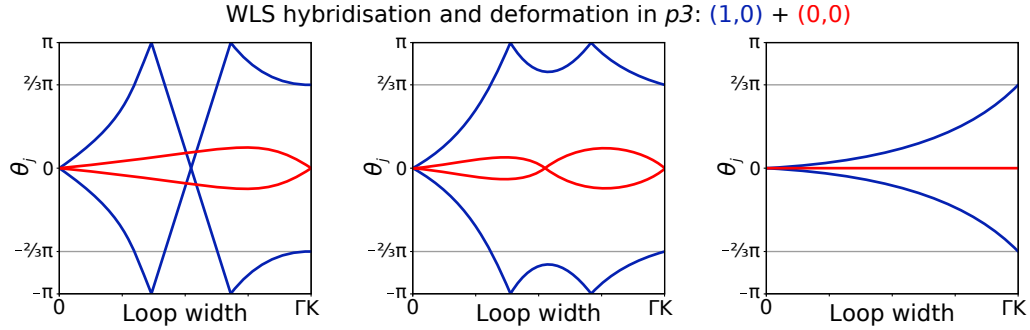

Figure B.1. Sketch of an allowed hybridisation and deformation process of a WLS with $(w_{\mathrm{FKM}}, w_\pi) = (1, 0)$ (blue) in the presence of a second, trivial $(0, 0)$ (red) occupied Kramers pair. Importantly, the topological class remains the same throughout.

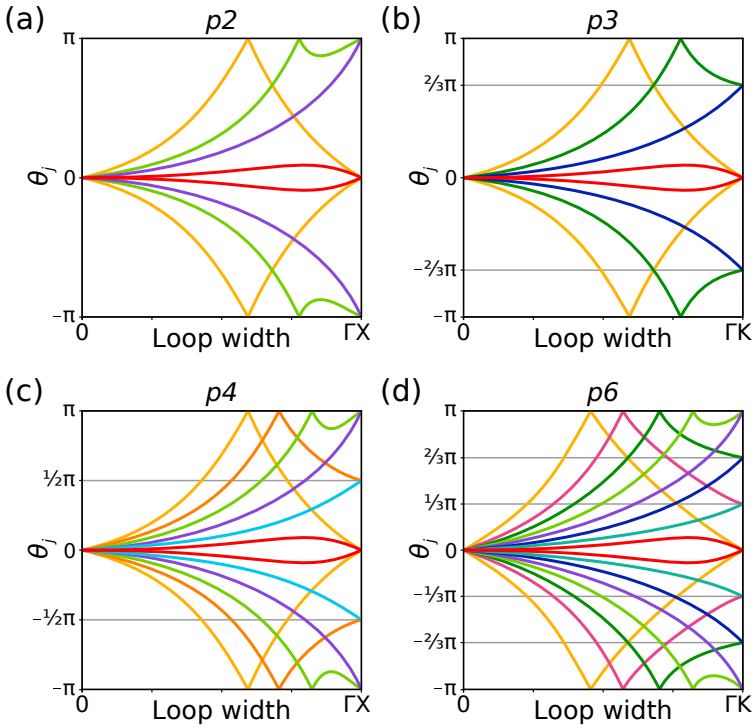

Figure B.2. Sketch of all elementary Wilson loop spectra for systems with TRS and n-fold rotational symmetry, determined by concentric Wilson loops that expand from Γ to covering $1/n^{\text{th}}$ of the BZ. All pure rotation wallpaper groups are represented here, with n equal to (a) 2, (b) 3, (c) 4 and (d) 6. The horizontal grey lines indicate allowed endpoints of the spectra, which correspond to $2\pi/n$.

Appendix C: A second example in $p2$

In the main text, we have demonstrated the evaluation of our new invariant in a class AII system with two-fold rotational symmetry (wallpaper group $p2$). We demonstrate a second example of this in Fig. C.1, for the C_2-symmetric Hamiltonian used in Ref. [3], where we compare the linear WLS to a concentric WLS over half the Brillouin zone, and it is clear our new invariant is non-trivial ($w_\pi = 1$). While this model was previously described to host "fragile" topology [3], we note that our new invariant is stable upon the addition of trivial Kramers pair.

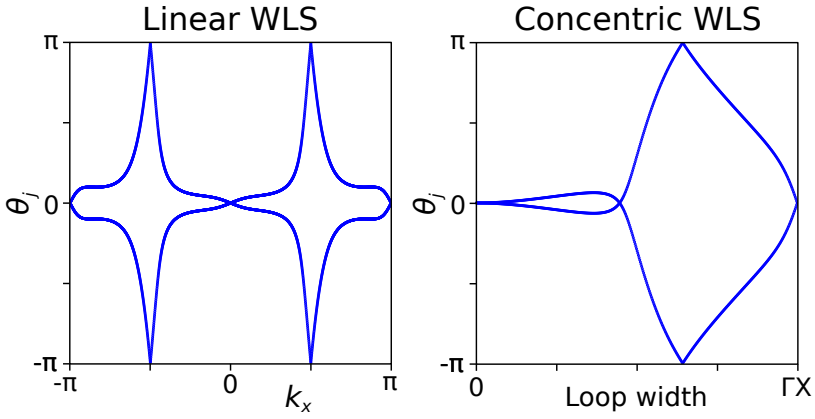

Figure C.1. A comparison of the linear and concentric WLS of the two-fold rotationally symmetric model considered in Ref. [3]. The concentric WLS indicates the FKM and new topological invariants, which along with two independent LBO invariants completes the classification: $(w_{\text{FKM}}, w_\pi, w_{\text{LBO}_x}, w_{\text{LBO}_y}) = (0, 1, 0, 0)$.

Appendix D: Ribbon bandstructures of the extended Haldane model

To determine whether the three topological phases of the extended Haldane model (as described in the main text) host edge states, we consider two types of ribbon configurations. The honeycomb lattice structure of the system allows for two different (clean) terminations, commonly known as armchair or zigzag edges, which are constructed by breaking translational symmetry along the x or y directions, respectively. This distinction is important to make, because the two atoms in the unit cell (A and B) have different on-site energies ($\pm m$). While armchair edges host equal numbers of each of the A and B atoms on the edge, the two types of sites making up the zigzag edge will have different species of outermost atoms, breaking this sublattice symmetry. Figure D.1 shows numerically evaluated band structures for systems with both armchair and zigzag edges [9], where we considered widths of 49 and 28 unit cells respectively, so that the ribbons have equal real-space width when the lattice geometry is taken into account.

In all three topological phases, the bulk system is an insulator, while edge states should show up in the ribbon geometry as in-gap states. In Fig. D.1, the four states closest to $E = 0$ are highlighted in red. In the $\mathbf{w} = (0, 0)$ phase, these red states do not cross the gap and act like bulk states. For zigzag-edged ribbons, they become almost completely flat bands, which is likely due to charge localisation on the outermost atoms in the zigzag edges. This is made possible by the different on-site energies on A and B-type atoms in the unit cell. In contrast, the (1,0) phase

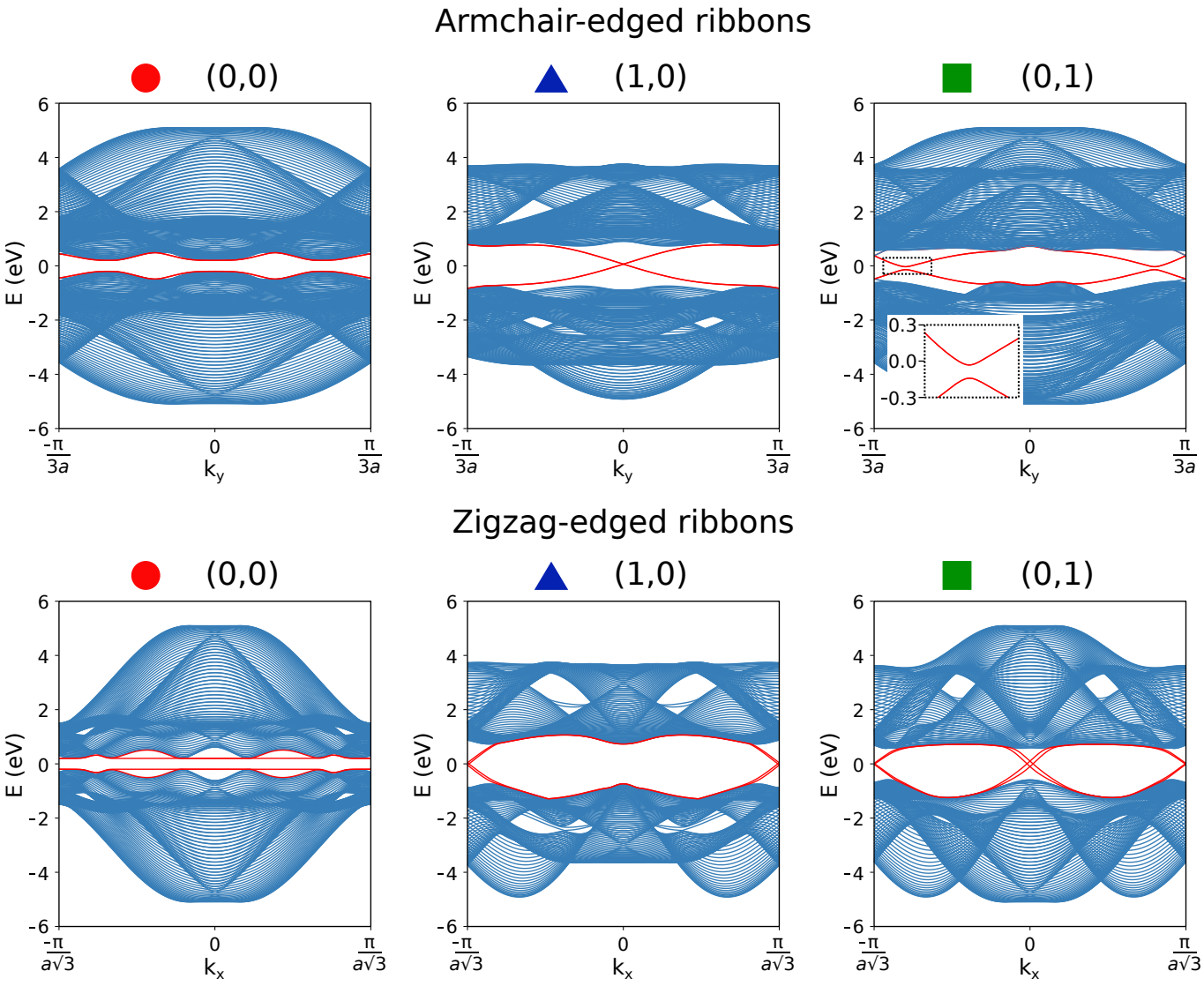

Figure D.1. Bandstructures for ribbons with armchair or zigzag edges, of the extended Haldane model with parameter values as indicated by the symbols in Fig. 2 in the main text. The different parameter choices correspond to three different topological phases, with the indicated topological indices. Highlighted in red are the four states closest to the Fermi level.

contains edge states crossing the band gap, as expected for a system with non-trivial FKM invariant. Note that these edge states are two-fold degenerate in the armchair-edged ribbons, while this degeneracy is broken in the zigzag-edged ribbons. Finally, in the (0,1) phase, we find that the in-gap armchair edge states become gapped, while the zigzag edge states remain. In a finite-sized hexagon with armchair edges (Fig. 4 in the main text), this phase hosts corner states whose energies can be tuned to fall within the spectral gap between the armchair edge states.

An interesting area to further explore would be the protection of edge states against gapping in the various ribbon geometries. For the $(1,0)$ phase, the armchair edge states form a two-fold degenerate crossing, while the breaking of sublattice symmetry in the zigzag-edged ribbon splits the edge states into two non-degenerate crossings. Each such crossing contains two edge states, localized on opposite edges of the ribbon. These crossings are thus protected from opening a gap by the suppression of their overlap due to the large real-space distance between edges. States in different crossings on the other hand, are time-reversed partners, and cannot scatter into one another without breaking time-reversal symmetry. These same constraints remain in the degenerate armchair-edged ribbons, so that edge states in the $(1,0)$ phase are topologically protected.

In the $(0,1)$ phase, the number of zero energy crossings is doubled as compared to the $(1,0)$ phase. In this case, each side of the ribbon hosts two pairs of edge states connected by time-reversal symmetry. If two states on the same side of the ribbon that are not time-reversed partners can be brought together in k_x-space, they can be gapped. This happens in the armchair geometry. For the zigzag-edged ribbon in Fig. D.1, states with the same real-space localization that are not time-reversed partners are still separated in momentum, and therefore not gapped. It may be possible to move the edge states crossings in k_x space by tuning model parameters until they meet and open a gap by hybridising. Similarly, the addition of impurities that break the translational symmetry along the ribbon edge and allow scattering without conserving k_x may also lead to a gap opening in the edge spectrum. In the presence of such a gap, it may be expected that corner charges could be stabilised also for finite hexagon-shaped systems with zigzag edges.

[1] R. Yu, X. L. Qi, A. Bernevig, Z. Fang, and X. Dai, Phys. Rev. B **84**, 075119 (2011).
[2] A. Bouhon, A. M. Black-Schaffer, and R.-J. Slager, Phys. Rev. B **100**, 195135 (2019).
[3] S. H. Kooi, G. van Miert, and C. Ortix, Phys. Rev. B **100**, 115160 (2019).
[4] B. Bradlyn, Z. Wang, J. Cano, and B. A. Bernevig, Phys. Rev. B **99**, 045140 (2019).
[5] A. Alexandradinata, X. Dai, and B. A. Bernevig, Phys. Rev. B **89**, 155114 (2014).
[6] H. C. Po, H. Watanabe, and A. Vishwanath, Phys. Rev. Lett. **121**, 126402 (2018).
[7] Y. Hwang, J. Ahn, and B.-J. Yang, Phys. Rev. B **100**, 205126 (2019).
[8] J. Kruthoff, J. de Boer, and J. van Wezel, Phys. Rev. B **100**, 075116 (2019).
[9] D. Moldovan, M. Anđelković, and F. Peeters, "pybinding v0.9.5: a Python package for tight- binding calculations," (2020).